

# A prediction for 25th solar cycle using visibility graph and Hathaway function

Eduardo Flández<sup>1\*</sup> and Víctor Muñoz<sup>1</sup>

<sup>1</sup>*Departamento de Física, Facultad de Ciencias, Universidad de Chile, Casilla 653, Santiago, Chile*

We apply a complex network approach to analyse the time series of five solar parameters, and propose an strategy to predict the number of sunspots for the next solar maximum, and when will this maximum will occur. The approach is based on the Visibility Graph (VG) algorithm, and a slightly modified version of it, the Horizontal Visibility Graph (HVG), which map a time series into a complex network. Various network metrics exhibit either an exponential or a scale-free behavior, and we find that the evolution of the characteristic decay exponents is consistent with variations of the sunspots number along solar cycles. During solar minimum, the sunspots number and the solar index time series have characteristic decay exponents that correlate well with the next maximum sunspots number, suggesting that they may be good precursors of the intensity of the next solar maximum. Based on this observation, we find that, based on current data, the algorithm predicts a number of 179 sunspots for cycle 25. Combining this with the Hathaway function, adjusted to yield such maximum sunspots number, we find that the maximum for solar cycle 25 will occur in December 2024/January 2025.

## I. INTRODUCTION

The number of sunspots is one of the main signatures of the variation of solar magnetic activity, having been recorded for centuries. It shows that solar activity exhibits an 11-year cycle, where the maximum of the cycle has the largest number of sunspots and solar flares [1–3], but although the most accepted explanation to date for the origin and dynamics of the solar magnetism is the dynamo theory [1, 4–7], modeling of the solar cycle remains a challenge. In particular regarding some specific features of the solar cycle: when will the next solar maximum occur, when will it start, how long it will last, and the maximum sunspots number, given their relevance to space weather parameters such as solar flare frequency and intensity, solar wind conditions, and geomagnetic activity.

Forecasting models based on concepts from nonlinear dynamics theory applied to experimental time series, such as embedding phase space, Lyapunov spectrum, and chaotic behavior, have been proposed [8]. There are also surface flux transport (SFT) models, that describe the transport of magnetic flux across the solar surface, modelling it as an advective-diffusive transport [9, 10], and models based on solar dynamo, based on a mean-field theory approach, where a system of coupled partial differential equations governs the evolution of the toroidal and poloidal components of the large-scale magnetic field [11, 12].

Also, various methods have been proposed to predict the solar cycle (see *e.g.* [13]), based on statistical correlations between solar and/or geomagnetic quantities.

The essential idea is that there exist historical correlations between solar activity indices during cycle minima and the following maxima. [14] If such correlations are found, then observing the sun during a certain min-

imum can provide information to forecast features of the next cycle. For instance, a regression technique has been proposed for predicting solar activity levels one year ahead [15], and functions which fit the sunspots number curve, based on two free parameters for each solar cycle: a starting time and an amplitude [16]. Various quantities have been proposed to use these correlations, in sunspot number records [17], in the Sun's polar magnetic field, and in geomagnetic indices [18].

Recently, the visibility graph technique has shown to be an interesting tool for time series analysis, as it provides a method to transform a time series into a complex network, whose metrics can be used to explore the statistical properties of the time series [19]. It has been used to characterize the light curves of pulsating variable stars [20], to study variations in solar activity along solar cycles [21, 22], to analyze solar wind velocities [23], and to study the statistical properties of solar flares [24, 25]. These works have shown that the metrics of the visibility graphs can be correlated to various stages of solar magnetic activity along the solar cycle.

Following these ideas, we propose that visibility graphs can provide a further means to find correlations between features of the solar minima and the next solar maxima, in the spirit of similar strategies based on the time series itself [13, 14, 26].

The paper is structured as follows. In Section II, the datasets utilized for the analysis are outlined. Then, in Sec. III the relevant complex network and visibility graph concepts are presented. Results are shown in Sec. IV, and they are discussed and summarized in Sec. V.

## II. DATA

We build complex networks using the time series of daily data for five parameters related to solar magnetic activity, from solar cycle 20 until June 11, 2023, corresponding to the ascending phase of SC 25. The chosen parameters are: Alfvén Mach number, proton flux,

---

\* eduardo.flandez@ug.uchile.cl

magnetic field, 10.7 cm radio flux and sunspots number, consistent with Ref. [27], in order to allow to compare with previous research. The respective time series with a cadence of one day are plotted in Fig. 1.

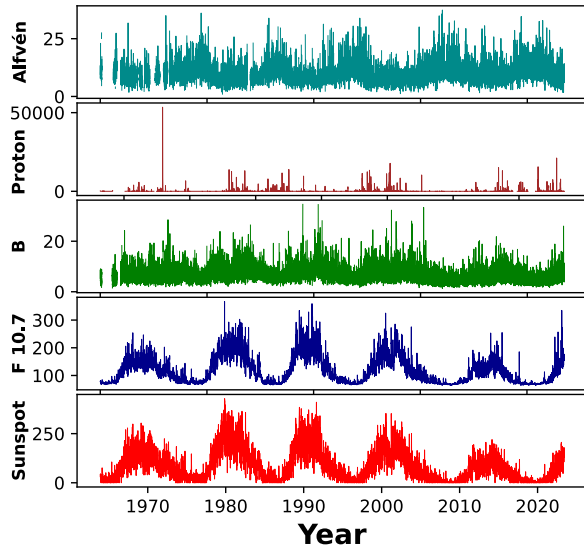


FIG. 1. Daily values for Alfvén Mach number, proton flux, solar magnetic field, F10.7 index and sunspot numbers, corresponding to solar cycles 20–24, and the beginning of 25.

Data have been taken from NASA Space Physics Data Facility (SPDF) (<https://omniweb.gsfc.nasa.gov/ow.html>). The Low Resolution OMNI (LRO) dataset is primarily a compilation of hourly-averaged, near-Earth solar wind magnetic field and plasma parameter data from various spacecraft in geocentric or Lagrange point 1 (L1) orbits, spanning from 1963 to the present ([https://omniweb.gsfc.nasa.gov/html/ow\\_data.html](https://omniweb.gsfc.nasa.gov/html/ow_data.html)). Additional details about the Alfvén Mach number, proton flux, and the F10.7 index are given below.

The Alfvén Mach number ( $M_A$ ) is the ratio between plasma velocity  $V$  and Alfvén velocity  $V_A$ , and has been used to model and characterize the space weather [28, 29]:

$$M_A = \frac{V}{V_A}. \quad (1)$$

In general, the shock speed should be included in the Mach number calculation, necessitating some additional assumptions. Since the bow shock typically remains in front of the Earth, assuming it is stationary is reasonable for long-term averages. With a stationary bow shock, the Mach number simplifies to the one described above.

Solar proton events (SPEs) are more frequent during solar maximum, typically caused by rapid coronal mass ejections. During these events, satellites face increased exposure to high-energy particles [30, 31]. Proton flux

data from various spacecraft, such as IMP and GOES, is available in OMNI and OMNI 2 databases, covering energies above key thresholds like 1, 10, and 60 MeV, with measurements spanning several decades from different missions (<https://satdat.ngdc.noaa.gov/sem/goes/data/avg>). Detailed information about the instrument and data can be found at [http://sd-www.jhuapl.edu/IMP/imp\\_index.html](http://sd-www.jhuapl.edu/IMP/imp_index.html) and <http://imp.ftccs.com>.

The solar spectral irradiance at 10.7 cm (F10.7, expressed in units of  $10^{-22} \text{Wm}^{-2} \text{Hz}^{-1}$ ) is used as an index of solar activity. Each F10.7 value represents the total emission at a wavelength of 10.7 cm from all sources present in the solar disk, measured over a period of one hour. Wavelengths in the 10 cm region are particularly effective for monitoring solar activity levels because emissions at these wavelengths are highly sensitive to conditions in the upper chromosphere and the base of the corona [32].

Based on each time series in Fig. 1, we will study their temporal variability along the four solar cycles under consideration, in order to derive parameters that may provide clues to predict when Solar Cycle 25 will occur. This will be achieved using complex networks, as explained in Sec. III.

### III. METHOD

As mentioned in Sec. I, some correlations between the value of solar or geomagnetic variables during solar minimum, and the number of sunspots at the following solar maximum have been found. This is related to the idea that the magnetic field at the Sun’s poles serves as a precursor for the next cycle. It has been shown that there is a linear correlation between the difference in the magnitude of north and south magnetic fields during solar minimum,  $\Delta B_{\text{poles}}$ , and the next maximum number of sunspots, so that when the difference between the north and south polar magnetic fields is higher, then the maximum number of sunspots is also higher. The Sun’s polar field difference  $\Delta B_{\text{poles}}$  has been one of the most reliable predictors of the last three cycles, since measurements have been available [26]. Based on the 24/25 cycle minimum in December 2019, the prediction indicates a maximum sunspot number of 120 for cycle 25 [26].

Another example is geomagnetic activity near cycle minima [33], which has the advantage of having more available data, namely for the last 13 sunspot cycles. This involves the *aa* geomagnetic index, which measures the amplitude of geomagnetic disturbances in nanoteslas (nT) from records of two geomagnetic stations, one in each of the Earth’s hemispheres. The higher the value of the *aa* index, the more intense the geomagnetic disturbance. It has been observed that the minimum of geomagnetic activity, as measured by the *aa* index, is correlated to the amplitude of the next cycle [34]. Using data for the 24/25 cycle minimum, this approach leads to a maximum sunspot number of 132 for cycle 25 [26].

Given the intrinsic nonlinearity of solar and space physics phenomena, there has been an increasing interest in using complex systems approaches to describe and model them, [35, 36] and gain new insights on issues such as the occurrence of geomagnetic storms [37] or the passage or magnetic structures in the solar wind [38]. Complexity approaches have also been applied to the problem of forecasting the solar cycle. In Ref. [27], an analysis of long memory processes in solar activity was made. They considered the same solar parameters as in Fig. 1, but for years 1976–2016. By applying a statistical test of persistence of solar activity using the Hurst exponent  $H$ , they determined the maximum number of sunspots to be  $102.8 \pm 24.6$ . Through simplex projection analysis, they forecasted that solar cycle 25 would begin in January 2021 and last until September 2031, with its maximum occurring in June 2024.

In our work, we intend to establish to what extent a complex network analysis can be used to predict features of the next solar maximum, based on the same parameters as in Ref. [27]. Complex networks have become a widely used strategy for studying complex systems, as they allow the abstraction of systems made up of a large number of interrelated components in a very general way. They have provided a useful approach to tackle various issues in space physics [39, 40], earthquakes analysis [41–47], atmospheric flows [48], and numerous other research areas (see for example Ref. [49]). Regarding solar activity, complex networks have been used to study time reversibility in turbulent states in solar wind simulations [50], to assess the probability of flares in solar active regions [51], to analyze solar magnetograms [52], characterize the sunspot time series [39], and more recently, to explore solar flare statistics [25, 53–55].

A network consists of vertices (nodes) connected by edges. Physically, nodes can represent entities that constitute a given system (people in a society, molecules in a solid, servers on the Internet, etc.), and connections can represent links or interactions between them (friendship relationships, electrical interactions, flow of data, etc.). If the connections in a network have an assigned orientation, the network is said to be directed. If the connections have no orientation, the network is undirected [56]. For this work, we construct a complex network using the visibility graph (VG) algorithm, which converts a time series into a graph. In this graph, each node represents a data point in the series, and two nodes are connected if both nodes can “see” each other (the straight line which joins both points lies above all intermediate data points [19]).

We also consider a variation of the above called the horizontal visibility algorithm (HVG), where visibility is given by horizontal lines [57]. Visibility graphs have been shown to be an interesting approach to extract statistical properties from time series, which can be in turn related to the underlying physical processes leading to such time series. For instance, it has been shown that the VG is able to distinguish between time series generated by fractal versus fractional brownian motion processes [58],

whereas the HVG can distinguish uncorrelated, or correlated stochastic processes [57]. This has led to various works which use VG/HVG techniques to characterize the physics which leads to the observed time series, such as unveiling correlations in earthquakes sequences [59], studying the degree of persistence in Brownian motion processes [58], screening of sleep disorders [60], quantifying irreversibility issues in physical processes [61] (such as interplate vs. intraplate seismicity [62]), discriminating between pulsation modes in variable stars [20], and following the evolution of solar magnetic activity [22, 39].

Based on these results, in this paper we study whether the VG approach can provide metrics which can, in turn, be correlated to solar magnetic activity and be used as precursors for the amplitude of the next solar cycle.

VG and HVG are determined for each of the time series in Sec. II. In order to define the graph, a time window of data must be selected, and two choices will be considered: the complete data set, and sliding windows. We construct undirected networks, whose metrics are then analyzed. Details are provided in Sec. IV.

#### IV. RESULTS

One of the simplest measures for a network is the degree  $k$  (number of connections per node). Despite its simplicity, the probability distribution of the degree  $P(k)$  can provide information about the underlying processes, revealing whether it is a random process or it follows some kind of preferential attachment [49], and various studies have shown the usefulness of the characteristic decay exponents at the tail of the distribution to characterize the topology of the complex network and its evolution [20, 22, 39, 44, 52, 63, 64].

Thus, we build a complex network via the VG algorithm, for each one of the five solar parameters in Sec. II, and study its degree distribution  $P(k)$ . Results show that distributions follow a power-law behavior, with characteristic exponent  $\gamma$ , both for the complete time series and for sliding windows (11-years wide, shifted by one year with respect to the previous one). This is consistent with previous works [19, 20].

However, in the spirit of previous works such as [39], a plot of  $\gamma$  as a function of the mean number of sunspots  $R$  for the corresponding time window is made, but it does not show a direct correlation for any of the five time series, as illustrated in Fig. 2.

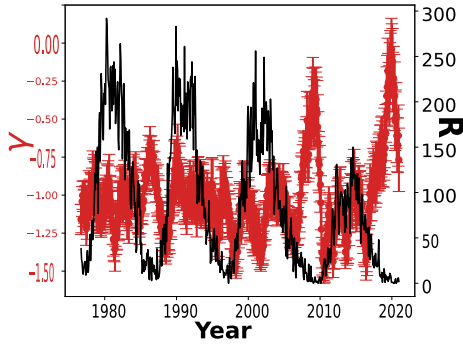


FIG. 2. Decay exponent  $\gamma$  for the degree distributions of visibility graphs, using 11-years moving windows of the sunspots time series. Red curve: decay exponent  $\gamma$ ; black curve: average sunspots number  $R$  during the time window.

We now repeat the previous analysis, but for the Horizontal Visibility Graph (HVG) algorithm [57]. The resulting degree distributions for each time series are exponential, with decay exponent  $\delta$ , which is consistent with previous works [19, 38, 39, 57, 65]. A semilog plot of the distributions, with their corresponding characteristic exponents and best fits are shown in Fig. 3.

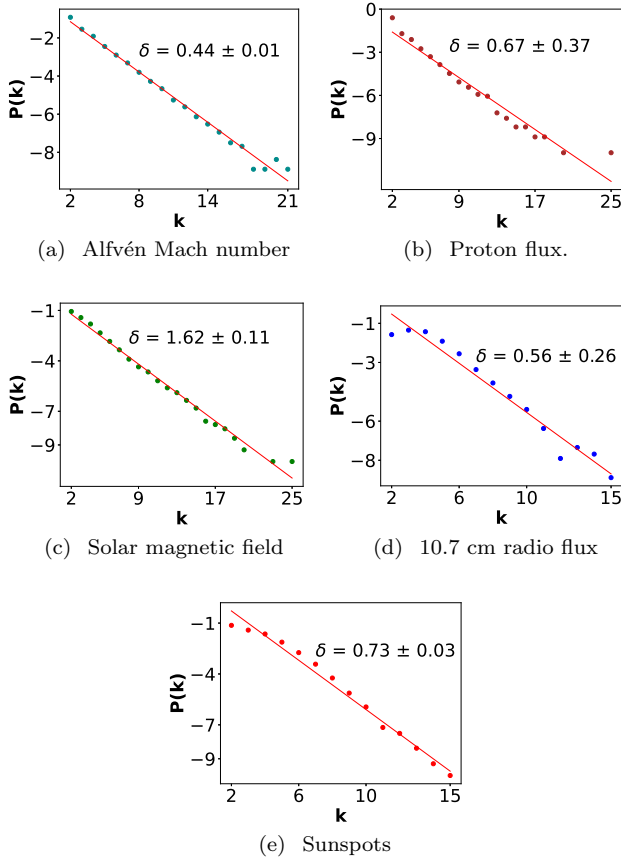


FIG. 3. Degree distributions for HVG, for each solar parameter in Fig. 1, in semilogarithmic scale.

The fit for the HVG algorithm (Fig. 3) turns out to be better than for the VG algorithm, being well represented by a function of the form  $e^{-\delta k}$ . This suggests that the HVG can be more useful than the VG in this case. The respective characteristic decay exponents are shown in Fig. 3, and in Table I.

Solar parameter	$\delta$
Alfvén Mach number	$0.44 \pm 0.01$
Proton flux	$0.67 \pm 0.37$
Magnetic field	$1.62 \pm 0.11$
10.7 cm radio flux	$0.56 \pm 0.26$
Sunspots	$0.73 \pm 0.03$

TABLE I. Characteristic exponent for each time series, obtained from linear fit for Fig. 3.

For the moving windows analysis, the plot of the decay exponent is shown in Fig. 4. In Fig. 4, we note that there is a periodic variation in the exponent  $\delta$  for the solar parameters that is consistent with the variation of the solar cycles, except for the proton flux.

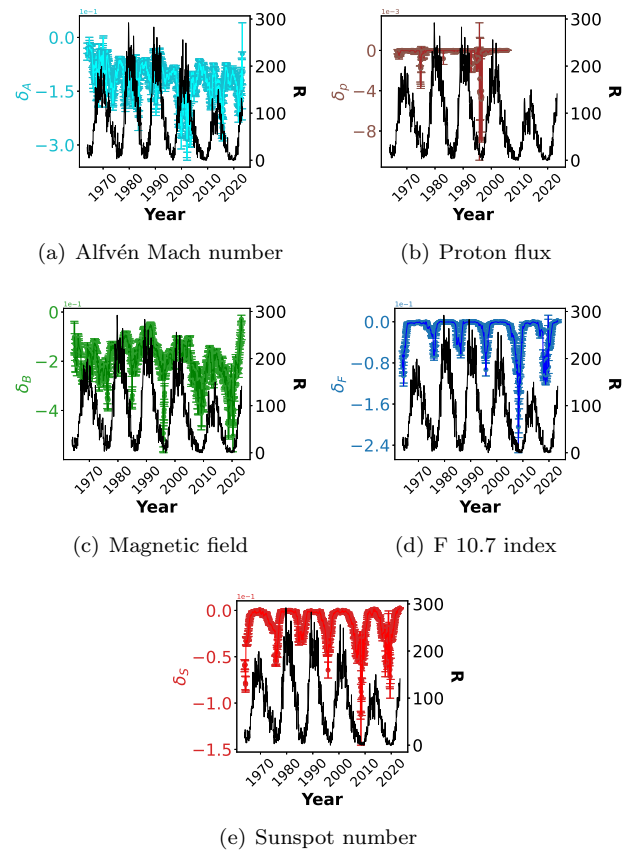


FIG. 4. Decay exponent  $\delta$  obtained from horizontal visibility graphs for 11-years wide time moving windows. Black curves: average sunspots number  $R$  during the time window.

The most interesting curves are found for the 10.7 cm radio flux and the sunspots curves, Figs. 4(d) and (e),

which show a clear anticorrelation with the sunspots number, where deeper minima in  $\delta$  occur before lower maxima of  $R$ . This is interesting, as it reminds similar correlations found in previous works on precursors based on completely different quantities, [26] as discussed in Sec. I. Thus, we will focus on those two solar parameters.

Following previous literature, in order to extract possible precursor information, we will smooth the selected parameters, the 10.7 radio flux and the sunspots number, from Fig. 4, by means of a Savitzky-Golay filter. The Savitzky-Golay filter, commonly used in signal processing, aims to reduce noise and improve the smoothness of signal trends. It achieves this by fitting a polynomial to each window of data, determined by the chosen polynomial degree and window size [66]. Smoothed curves are shown in Fig. 5.

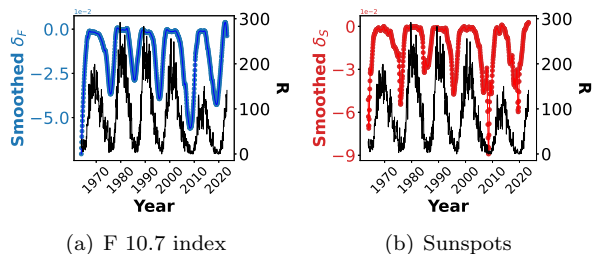


FIG. 5. Same as Fig. 4, but for smoothed curves for the  $\delta$  exponent.

Now we plot the maximum number of sunspots in the next solar maximum ( $R_{\max}$ ), versus the minimum value of  $\delta$  during a solar minimum ( $\delta_{\min}$ ), taken from the smoothed curves in Fig. 5. Results are shown in Fig. 6, including the corresponding linear fits.

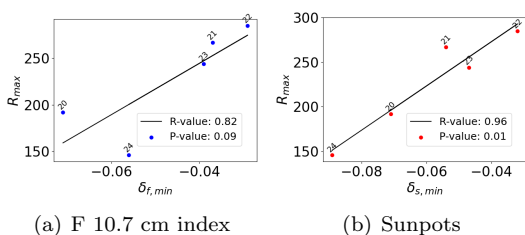


FIG. 6. Maximum sunspots number versus minimum  $\delta$  for each solar cycle, for solar index (blue dots) and for sunspot (red dots).

The linear fits are given by

$$R_{\max}^{\delta_f, \min} = 2755 \cdot \delta_{f, \min} + 355, \quad (2)$$

$$R_{\max}^{\delta_s, \min} = 2483 \cdot \delta_{s, \min} + 372, \quad (3)$$

for the solar index and the sunspots curves, respectively. The R-values are 0.82 for the F 10.7 cm index, and 0.96

for sunspots, whereas  $p$ -values is 0.09 for the solar index and 0.01 for sunspots. Based on these results, the prediction for the maximum number of sunspots for the next solar cycle is  $R_{\max}^{\delta_f, \min} = 160$  if the solar index curve is considered, and  $R_{\max}^{\delta_s, \min} = 179$  if the sunspots curve is considered.

We have used this method for the previous cycles in order to obtain an estimation of the accuracy of the proposed method. If the fits (2) and (3) hold, then Table II shows the predicted maximum number of sunspots, along with the official number.

TABLE II. For each solar cycle (SC) considered, the maximum number of sunspots  $R_{\max}$  according to the Solar Cycle Prediction Panel (SCPP), and the results given by our Eqs. (2) and (3).

SC	$R_{\max}$	$\delta_{f, \min}$	$R_{\max}^{\delta_f, \min}$	Error %	$\delta_{s, \min}$	$R_{\max}^{\delta_s, \min}$	Error %
20	157	-0.071	159	0.6	-0.071	196	1.3
21	233	-0.037	253	23.9	-0.054	238	7.9
22	213	-0.029	275	5.8	-0.032	293	22.5
23	180	-0.039	248	10	-0.047	255	27.4
24	116	-0.056	201	8.7	-0.089	151	42.3
25	-	-0.043	160	-	-0.059	179	-

Since this strategy consists of correlating the values of one parameter during solar minimum, to the values of another parameter during the following solar maximum, each cycle provides one point, which affects the statistics. A similar issue is found in related works. For instance, four points are also used in Refs. [14, 67, 68], where the Polar Field Strength is used. Consequently, correlation coefficients tend to be low. In Ref. [14], a  $cc = 0.676$  for the correlation between sunspots number during solar minimum and during solar maximum, and Ref. [69] has  $cc = 0.72$  for the correlation between magnetic flux at the poles during solar minima, and the amplitude of the next solar maximum.

Statistics can be improved by considering previous solar cycles, but this is possible only for the sunspots number. As mentioned above, we are interested in comparing with recent work using the same parameters as us, which sets the time window to be studied.

The Solar Cycle Prediction Panel predicts that the solar maximum would be in July 2025 ( $\pm 8$  months), reaching a maximum number of sunspots of 115. They predicted that this would be a below-average solar cycle. Our result of  $R_{\max}^{\delta_s, \min} = 179$  is closer to the behavior of the current solar cycle than the 115 predicted by the Panel. Our result is consistent with what is mentioned in Ref. [70], where they identified the so-called “termination” events that mark the end of each cycle. Based on this, they extracted a relationship between the temporal spacing of the termination events and the magnitude of the cycles [71], leading to the conclusion that Solar Cycle 25 should have a magnitude greater than that proposed by the Solar Cycle Prediction Panel. On the other hand,

in Ref. [72],  $R_{\max} = 175$  is proposed, which is also close to what we obtain.

We can also estimate the date for the next solar maximum, based on previous work by Hathaway [16], where the number of sunspots as a function of time  $R(t)$  is adjusted with

$$R(t) = \frac{A(t - t_0)^3}{\exp[(t - t_0)^2/B^2] - C}, \quad (4)$$

where  $A$ ,  $B$ ,  $C$ , are adjustable parameters, and  $t_0$  is an estimation of the time where the last solar minimum occurred.  $A$ ,  $B$ ,  $C$  are adjusted to fit the curve so that it starts at  $R(t_0) = 0$ , and its maximum value is  $R_{\max}$ . In Ref. [16], it is assumed that  $t_0$  is 5.15 months before December 2019, and adjustable parameters are  $A = 0.00170 \pm 0.00040$ ,  $B = 14.2 + 8.33 \times A^{-1/4}$ , and  $C = 0.42$ .

We will use the same model, Eq. (4), but will adjust  $C$  and  $t_0$  to match our  $R_{\max} = 179$  prediction. Proceeding in this way, we obtain that the next solar maximum, for cycle 25, will occur in December 2024/January 2025. Figure 7 shows the predicted curve Eq. (4) resulting from our parameters (red), along with the observed sunspots number for the current cycle (green), to show the agreement between the curves so far.

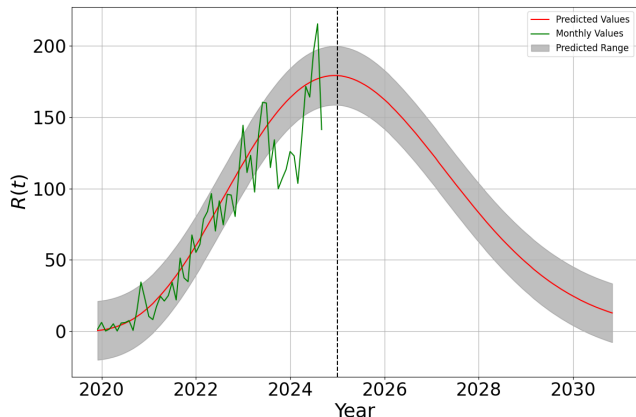


FIG. 7. Sunspots number forecast for solar cycle 25. Maximum number of sunspots is 179, and occurs in December 2024/January 2025.

It is interesting to notice that our results are consistent with Ref. [70], but using a different approach.

## V. SUMMARY

We analyze the time series of five solar parameters through complex network analysis. To do this, we construct a complex network using the visibility graph and the horizontal visibility graph algorithms, which convert

the time series into a graph, where each node corresponds to a data point in the series, and two nodes are connected if visibility exists between the corresponding data points. For networks built with the VG algorithm, the degree distribution  $P(k)$  has a power-law decay, whereas for networks built with HVG it has an exponential decay, a result which is consistent with previous works.

A moving windows analysis show that the decay exponent  $\delta$  for the HVG exhibits a correlation with the solar cycle, but only for the sunspots and the F 10.7 time series: the value of  $\delta$  during a minimum of the solar cycle is lower when the number of sunspots during the following solar maximum is higher. Fitting this to a linear trend, and using the value of  $\delta$  for the last solar minimum, a maximum number of sunspots of 179 is found for the next solar maximum. Adjusting the Hathaway function [13, 16, 26] to reach this maximum number, yields that the maximum of solar cycle 25 will occur in December 2024/January 2025.

Several improvements can be made to this approach. The same parameters as in Ref. [27] have been used, which limits the analysis to the last 5 solar cycles, due to data availability. This, in turns, leads to lower statistics. As long as measurements continue, further data can be gathered, and the quality of the correlations could be better assessed. For sunspots, however, there are longer records, and the method can be applied for a larger number of solar cycles, although no comparison with other time series is possible. Besides, in this work we have only taken the simplest metric, the degree distribution, but various other metrics could be considered, as previous works have shown that the clustering coefficient, betweenness centrality, or Gini coefficients [20, 22, 52] have shown to be useful in describing variations in solar activity.

Previous works have proposed similar strategies, based on correlations between physical parameters at solar minimum and the next solar maximum, to forecast features of the solar cycle. Our work follows these ideas, but with a different, complex network approach, yielding results which are consistent with existing literature, and suggesting a new path to explore in future research.

## VI. ACKNOWLEDGMENTS

We thank the Space Physics Data Facility, NASA/Goddard Space Flight Center.

## VII. FUNDING

This research was funded by FONDECyT grant number 1242013 (V.M.), and supported by ANID PhD grant number 21210996 (E.F.)

- 
- [1] C. J. Schrijver and G. L. Siscoe, editors, *Heliophysics: Plasma Physics of the Local Cosmos* (Cambridge Core, 2013).
- [2] P. A. Sturrock, *Physics of the Sun. Volume II: The Solar Atmosphere* (Springer, 2013).
- [3] C. J. Schrijver and G. L. Siscoe, editors, *Heliophysics: Evolving Solar Activity and the Climates of Space and Earth* (Cambridge Core, 2010).
- [4] P. Charbonneau, *Ann. Rev. Astron. Astrophys.* **52**, 251 (2014).
- [5] M. Aschwanden, *Physics of the Solar Corona: An Introduction with Problems and Solutions* (Springer, 2005).
- [6] Y. Kamide and A. C.-L. Chian, editors, *Handbook of the Solar-Terrestrial Environment* (Springer-Verlag, 2007).
- [7] K. R. Lang, *The Sun from Space* (Springer, 2009).
- [8] S. Sello, *Astron. Astrophys.* **377**, 312 (2001).
- [9] A. R. Yeates, M. C. Cheung, J. Jiang, K. Petrovay, and Y.-M. Wang, *Space Sci. Rev.* **219**, 31 (2023).
- [10] J. Jiang, D. Hathaway, R. Cameron, S. Solanki, L. Gizon, and L. Upton, *Space Sci. Rev.* **186**, 491 (2014).
- [11] R. Cameron, M. Dikpati, and A. Brandenburg, *Space Sci. Rev.* **210**, 367 (2017).
- [12] P. Charbonneau, *Liv. Rev. Solar Phys.* **2**, 2 (2005).
- [13] D. H. Hathaway, R. M. Wilson, and E. J. Reichmann, *J. Geophys. Res.* **104**, 22375 (1999).
- [14] K. Petrovay, *Liv. Rev. Solar Phys.* **17**, 2 (2020).
- [15] A. G. McNish and J. V. Lincoln, *EOS, Trans. Am. Geophys. Union* **30**, 673 (1949).
- [16] D. H. Hathaway, R. M. Wilson, and E. J. Reichmann, *Solar Phys.* **151**, 177 (1994).
- [17] R. M. Wilson, D. H. Hathaway, and E. J. Reichmann, *J. Geophys. Res.* **103**, 6595 (1998).
- [18] J. Feynman, *J. Geophys. Res.* **87**, 6153 (1982).
- [19] L. Lacasa, B. Luque, F. Ballesteros, J. Luque, and J. C. Nuno, *Proc. Nat. Acad. Sci.* **105**, 4972 (2008).
- [20] V. Muñoz and N. E. Garcés, *PLoS ONE* **16**, e0259735 (2021).
- [21] Y. Zou, R. V. Donner, N. Marwan, M. Small, and J. Kurths, *Nonlinear Proc. Geophys.* **21**, 1113 (2014).
- [22] T. Zurita-Valencia and V. Muñoz, *Entropy* **25**, 342 (2023).
- [23] V. Suyal, A. Prasad, and H. P. Singh, *Solar Phys.* **289**, 379 (2013).
- [24] Z. G. Yu, V. Anh, R. Eastes, , and D.-L. Wan, *Nonlinear Proc. Geophys.* **19**, 657 (2012).
- [25] S. Taran, E. Khodakarami, and H. Safari, *Adv. Space Res.* **70**, 2541 (2022).
- [26] D. H. Hathaway, *Liv. Rev. Solar Phys.* **7**, 1 (2010).
- [27] A. K. Singh and A. Bhargawa, *ass* **362**, 199 (2017).
- [28] C. A. Maguire, E. P. Carley, J. McCauley, and P. T. Gallagher, *Astron. Astrophys.* **633**, A56 (2020).
- [29] P. Hartigan and A. Wright, *Astrophys. J.* **811**, 12 (2015).
- [30] G. H. Nakano and H. H. Heckman, *Phys. Rev. Lett.* **20**, 806 (1968).
- [31] D. J. Williams and C. O. Bostrom, *J. Geophys. Res.* **74**, 3019 (1969).
- [32] K. F. Tapping, *Space Weather* **11**, 394 (2013).
- [33] A. I. Ohl, *Soln. Dannye* **12**, 84 (1966).
- [34] K. Schatten, D. J. Myers, and S. Sofia, *Geophys. Res. Lett.* **23**, 605 (1996).
- [35] M. J. Aschwanden, *et al.*, *Space Sci. Rev.* **198**, 47 (2016).
- [36] R. O. Dendy, S. C. Chapman, and M. Paczuski, *Plasma Phys. Controlled Fusion* **49**, A95 (2007).
- [37] M. Domínguez, V. Muñoz, and J. A. Valdivia, *J. Geophys. Res.* **119**, 3585 (2014).
- [38] V. Muñoz, M. Domínguez, J. A. Valdivia, S. Good, G. Nigro, and V. Carbone, *Nonlinear Proc. Geophys.* **25**, 207 (2018).
- [39] Y. Zou, M. Small, Z. Liu, and J. Kurths, *New J. Phys.* **16**, 013051 (2014).
- [40] S. Lu, H. Zhang, X. Li, Y. Li, C. Niu, X. Yang, , and D. Liu, *Nonlinear Proc. Geophys.* **25**, 233 (2018).
- [41] S. Abe and N. Suzuki, *Europhys. Lett.* **65**, 581 (2004).
- [42] S. Abe and N. Suzuki, *Nonlinear Proc. Geophys.* **13**, 145 (2006).
- [43] S. Abe, D. Pastén, and N. Suzuki, *Physica A* **390**, 1343 (2011).
- [44] D. Pastén, F. Torres, B. Toledo, V. Muñoz, J. Rogan, and J. A. Valdivia, *Pure Appl. Geophys.* **173**, 2267 (2016).
- [45] S. Abe, D. Pastén, V. Muñoz, and N. Suzuki, *Chinese Science Bulletin* **56**, 3697 (2011).
- [46] D. Pastén, Z. Czechowski, and B. Toledo, *Chaos* **28**, 083128 (2018).
- [47] D. Pastén, F. Torres, B. Toledo, V. Muñoz, and J. A. Valdivia, *Physica A* **491**, 445 (2018).
- [48] A. K. Charakopoulos, G. A. Katsouli, and T. E. Karakassidis, *Physica A* **495**, 436 (2018).
- [49] R. Albert and A.-L. Barabási, *Rev. Mod. Phys.* **74**, 47 (2002).
- [50] B. Acosta-Tripailao, D. Pastén, and P. S. Moya, *Entropy* **23**, 470 (2021).
- [51] F. Daei, H. Safari, and N. Dadashi, *Astrophys. J.* **845**, 36 (2017).
- [52] V. Muñoz and E. Flández, *Entropy* **24**, 753 (2022).
- [53] A. Najafi, A. H. Darooneh, A. Gheibi, and N. Farhang, *Astrophys. J.* **894**, 66 (2020).
- [54] A. Gheibi, H. Safari, and M. Javaherian, *Astrophys. J.* **847**, 115 (2017).
- [55] N. Lotfi, M. Javaherian, B. Kaki, A. H. Darooneh, and H. Safari, *Chaos* **30**, 043124 (2020).
- [56] M. E. J. Newman, *Phys. Rev. E* **95**, 108701 (2005).
- [57] B. Luque, L. Lacasa, F. Ballesteros, and J. Luque, *Phys. Rev. E* **80**, 046103 (2009).
- [58] L. Lacasa, B. Luque, J. Luque, and J. C. Nuño, *Europhys. Lett.* **86**, 30001 (2009).
- [59] S. Kundu, A. Opris, Y. Yukutake, and T. Hatano, *Frontiers Phys.* **9**, 656310 (2021).
- [60] R. Li, W. Li, K. Yue, and Y. Li, *Biomed. Signal Proc. Control* **86**, 104966 (2023).
- [61] L. Lacasa, A. Nuñez, É. Roldán, J. M. R. Parrondo, and B. Luque, *Eur. Phys. J. B* **85**, 217 (2012).
- [62] L. Telesca, D. Pastén, and V. Muñoz, *Pure Appl. Geophys.* **177**, 4755 (2020).
- [63] A.-L. Barabási and R. Albert, *Science* **286**, 509 (1999).
- [64] S. Guillier, V. Muñoz, J. Rogan, R. Zarama, and J. A. Valdivia, *Physica A* **467**, 465 (2016).
- [65] B. Kaki, N. Farhang, and H. Safari, *SIAM Review* **12**, 16835 (2022).
- [66] W. H. Press and S. A. Teukolsky, *Comput. Phys.* **4**, 669 (1990).
- [67] B. Benson, W. D. Pan, A. Prasad, G. A. Gary, and Q. Hu, *Solar Phys.* **295**, 65 (2020).

- [68] G. M. Brown, *Mon. Not. R. Astron. Soc.* **174**, 185 (1976).
- [69] D. Nandy, *Solar Phys.* **296**, 54 (2021).
- [70] S. W. McIntosh, S. Chapman, R. J. Leamon, R. Egeland, and N. W. Watkins, *Solar Phys.* **295**, 163 (2020).
- [71] R. J. Leamon, S. W. McIntosh, S. C. Chapman, and N. W. Watkins, *Solar Phys.* **295**, 36 (2020).
- [72] K. Li, W. Feng, and F. Li, *J. Atmos. Sol. Terr. Phys.* **135**, 72 (2015).